Identification of a Novel Noncatalytic Bicarbonate Binding Site in Eubacterial β-Carbonic Anhydrase

Jeff D. Cronk,*,‡ Roger S. Rowlett,*,§ Kam Y. J. Zhang,|| Chingkuang Tu,⊥ James A. Endrizzi,# Joseph Lee,§ Peter C. Gareiss,§ and Jeffrey R. Preiss§

Department of Chemistry, Gonzaga University, 502 East Boone Avenue, Spokane, Washington 99258, Department of Chemistry, Colgate University, 13 Oak Drive, Hamilton, New York 13346, Department of Pharmacology and Therapeutics, University of Florida College of Medicine, Gainesville, Florida 32610, Fred Hutchinson Cancer Research Center, 1100 Fairview Avenue North, Seattle, Washington 98109, and Department of Molecular and Cellular Biology, University of California, Davis, California 95616

Received November 6, 2005; Revised Manuscript Received February 4, 2006

ABSTRACT: The structures of β class carbonic anhydrases (β-CAs) determined so far fall into two distinct subclasses based on the observed coordination of the catalytic zinc (Zn^{2+}) ion. The subclass of β-CAs that coordinate Zn^{2+} tetrahedrally with four protein-derived ligands is represented by the structures of orthologues from *Porphyridium purpureum*, *Escherichia coli*, and *Mycobacterium tuberculosis*. Here we present the structure of an additional member of that subclass, that from *Haemophilus influenzae*, as well as detailed kinetic analysis, revealing the correspondence between structural classification and kinetic profile for this subclass. In addition, we identify a unique, noncatalytic binding mode for the substrate bicarbonate that occurs in both the *H. influenzae* and *E. coli* enzymes. The kinetic and structural analysis indicates that binding of bicarbonate in this site of the enzyme may modulate its activity by influencing a pH-dependent, cooperative transition between active and inactive forms. We hypothesize that the two structural subclasses of β-CAs may provide models for the proposed active and inactive forms of the *H. influenzae* and *E. coli* enzymes.

Carbonic anhydrase (carbonate hydrolyase, EC 4.2.1.1) is a zinc metalloenzyme that catalyzes the reversible interconversion of CO_2 and bicarbonate:

$$CO_2 + H_2O \leftrightarrows HCO_3^- + H^+ \quad (1)$$

Six classes of convergently evolved forms of CA[1] have been described to date. The α-form is found in animals and some eubacteria (*1*); a γ-form is represented in an archaebacterium (*2*); there are two diatom forms, δ (*3*) and ζ (*4*), the latter of which is apparently a cadmium metalloenzyme; and finally a carboxysome form (ϵ) has been reported (*5*). The remaining form of CA (β) is widely distributed in plants and eubacteria (*6*). The X-ray crystallographic structures determined for β-CAs reveal two distinct zinc coordination spheres. In the enzymes from *Pisum sativum* (*7*), *Methanobacterium thermoautotrophicum* (*8*), and *Mycobacterium tuberculosis* Rv1284 (*9*), the active site zinc ion is coordinated by one histidine and two cysteine residues, with a fourth coordination site occupied by water or a substrate analogue. In contrast, in the enzymes from *Porphyridium purpureum* (*10*), *Escherichia coli* (*11*), and *M. tuberculosis* Rv3588c (*9*) the active site water molecule has been replaced by an aspartate side chain, forming a noncanonical CA active site. The latter group of CAs is characterized by little or no CO_2 hydration activity at pH values less than 7.0, compared to the former group.

The nature of the relationship between these two subclasses of β-CA poses an interesting problem. Do the different coordination spheres in these β-CA subclasses imply that each has a fundamentally different catalytic mechanism? Or do these two structural variants of β-CA represent alternate conformations of the protein that are the hallmarks of a regulatory process? Direct evidence to support either of these alternatives has thus far been lacking. For example, all carbonic anhydrases kinetically characterized to date indicate noncooperative, Michaelis−Menten behavior despite the fact that, among the various CA classes, a wide variety of homooligomeric forms are observed. However, no members of the *P. purpureum*-like β-CAs have been rigorously kinetically characterized.

To help to address these issues, and to further define the kinetic profile of this structural subclass, we report here the crystallographic structure determination and kinetic charac-

* Address correspondence to these authors. J.D.C.: telephone, (509) 323-6627; fax, (509) 323-5804; e-mail, cronk@gonzaga.edu. R.S.R.: telephone, (315) 228-7245; fax, (315) 228-7935; e-mail, rrowlett@mail.colgate.edu.

‡ Gonzaga University.

§ Colgate University.

|| Fred Hutchinson Cancer Research Center. Present address: Plexxikon, Inc., 91 Bolivar Drive, Berkeley, CA 94710.

⊥ University of Florida College of Medicine.

University of California, Davis.

[1] Abbreviations: CA, carbonic anhydrase; ECCA, *Escherichia coli* β-carbonic anhydrase; HICA, *Haemophilus influenzae* β-carbonic anhydrase; PSCA, *Pisium sativum* β-carbonic anhydrase; EXAFS; extended X-ray absorption fine structure; SDS−PAGE, sodium dodecyl sulfate−polyacrylamide gel electrophoresis; PCR, polymerase chain reaction; TB medium, Terrific broth medium; LB medium, Luria−Bertani medium; IPTG, isopropyl β-D-thiogalactoside; DEAE, diethylaminoethyl; HEPES, 4-(2-hydroxyethyl)piperazineethanesulfonic acid; ICP-OES, inductively coupled plasma−optical emission spectroscopy; EDTA, *N*,*N*,*N*′-ethylenediaminetetraacetic acid; PEG-400, poly(ethylene glycol) 400; sAC, soluble adenylyl cyclase.

10.1021/bi052272q CCC: $33.50 © 2006 American Chemical Society
Published on Web 03/17/2006

terization of the β-CA from *Haemophilus influenzae* (HICA). We also report structural evidence for a noncatalytic bicarbonate binding site in the *E. coli* (ECCA) and *H. influenzae* enzymes. For bicarbonate dehydration at chemical equilibrium, HICA exhibits substrate inhibition. In addition, this enzyme exhibits highly cooperative pH−rate profiles both at steady-state and at chemical equilibrium. These data suggest that bicarbonate has a role in the allosteric regulation of activity of both ECCA and HICA, and potentially other members of the β-CA class.

EXPERIMENTAL PROCEDURES

Expression and Purification of Recombinant Enzymes. Recombinant ECCA was prepared as described previously (*12*). The entire gene encoding for HICA was PCR-amplified from plasmid obtained from clone HI1301 (American Type Culture Collection) using the oligonucleotide primers pHI1X (5′-TGCCCATGGATAAAATTAAACTCTTT-3′) and pHI2X (5′-TGCCTGCAGTTATTATGTATTTTCAAGATG-3′) which contain *Nco*I and *Pst*I restriction sites, respectively (underlined). The resulting PCR product was cloned into the *Nco*I and *Pst*I sites of pTrc99a, yielding the expression vector pHICA. The HICA coding sequence was verified by DNA sequencing (BigDye 2.0, PE Biosystems) using an ABI310 capillary electrophoresis sequencer (PE Biosystems). The HICA coding sequence of pHICA conforms to the expected coding sequence of HICA (GenBank NC_007146).

HICA was overexpressed by inoculating 1 L of TB medium supplemented with 1 mM $ZnSO_4$ and 100 μg/mL ampicillin with an overnight culture of *E. coli* (JM109) harboring pHICA. After growth at 37 °C with shaking to an OD_{600} of 0.6−1.0 (about $3^1/_2$ h), the culture was induced with 0.2 mM IPTG and shaken overnight at 37 °C. Cells were harvested by centrifugation at 8000*g* for 10 min, resuspended in 40 mL of buffer A3 (20 mM Tris-HCl, 10 μM EDTA, pH 8.00), and subjected to lysis in a BeadBeater (Biospec). The supernatant was clarified by centrifugation at 48000*g* for 45 min, loaded onto a 26 × 100 mm Q-Sepharose fast-flow column (Amersham) at 4 mL/min, washed with 3 column volumes of buffer A3 containing 150 mM NaCl, and eluted with 3 column volumes of buffer A3 containing 300 mM NaCl. Solid $(NH_4)_2SO_4$ was added to the pooled eluate to bring it to 1.0 M, and this solution was loaded onto a 16 × 100 mm butyl-Sepharose fast-flow column (Amersham) at 4 mL/min, washed with 3 column volumes of buffer A3 containing 900 mM $(NH_4)_2SO_4$, and eluted with 2 column volumes of buffer A3 containing 525 mM $(NH_4)_2SO_4$. Pooled eluate was concentrated to 2 mL using centrifugal ultrafiltration (MacroSep, 30K MWCO; Filtron) and applied to a 16 × 600 mm Superdex 200 column (Amersham) equilibrated with buffer A3 containing 100 mM NaCl. This column was eluted at 1 mL/min with the same buffer, and the major protein peak fractions were pooled. Purified protein was concentrated by centrifugal ultrafiltration to 500 μL and stored at 4 °C.

Active enzyme concentrations for both ECCA and HICA were determined by ICP-OES for Zn at 213.856 nm using a Perkin-Elmer Optima SC 3000.

Steady-State Kinetics Methods. Saturated solutions of CO_2 were prepared by bubbling CO_2 gas into water in a vessel maintained at 25 ± 0.1 °C, and dilutions were prepared in the absence of air by coupling two gastight syringes as described by Khalifah (*13*). CO_2 concentrations were calculated on the basis of a 33.8 mM saturated solution at 25 °C (*14*).

All steady-state kinetic measurements were made at 25 °C using a Hi-Tech SF-61DX2 stopped-flow spectrophotometer. Initial rates of CO_2 hydration were measured using the changing pH-indicator method described previously (*13*, *15*, *16*). All stopped-flow kinetic studies were carried out in the presence of 250 mM Na_2SO_4, which was required for maximum enzyme stability and activity in dilute solution. Values of k_{cat} and K_m were determined by nonlinear least-squares fits to v/[E] vs [CO_2] data using Origin 6.0 (Microcal). The kinetic constants k_{cat} and k_{cat}/K_m are reported here on a per subunit basis.

Oxygen-18 Exchange Kinetics Methods. The rate of exchange of ^{18}O between species of CO_2 and water (eqs 2 and 3) is catalyzed by carbonic anhydrase (*17*):

$$HCOO^{18}O^- + EZnH_2O \leftrightarrows EZnHCOO^{18}O^- + H_2O \leftrightarrows CO_2 + EZn^{18}OH^- + H_2O \quad (2)$$

$$EZn^{18}OH^- + BH^+ \leftrightarrows H^+ EZn^{18}OH^- + B \leftrightarrows EZn^{18}OH_2\ (+H_2O) \leftrightarrows EZnOH_2 + H_2{}^{18}O \quad (3)$$

Using an Extrel EXM-200 mass spectrometer with a membrane permeable to gases, we measured the isotopic exchange of ^{18}O shown in eqs 2 and 3 at chemical equilibrium and 25 °C (*17*). Solutions contained 250 mM Na_2SO_4 for maximum enzyme stability and activity. No added buffer species were present.

This method determines two rates in the catalytic pathway (*17*). The first, defined as R_1, is the rate of interconversion of CO_2 and HCO_3^- at chemical equilibrium. The pH dependence of R_1 is typically described by the equation (*18*):

$$\frac{R_1}{[E]} = \frac{R_1^{max}}{(1 + K_{Zn}/[H^+])(1 + [H^+]/K_{CO_2})} \quad (4)$$

where R_1^{max} is the maximal value of R_1, K_{Zn} is the apparent acid dissociation constant of enzyme-bound Zn-OH_2, and K_{CO_2} is the apparent acid dissociation constant of CO_2.

This method also determines a second rate, R_{H_2O}, which is the rate of release from the enzyme of water labeled with ^{18}O. A proton from a donor group (BH^+ in eq 3) converts zinc-bound ^{18}O-labeled hydroxide to zinc-bound ^{18}O-labeled water, which readily exchanges with and is irreversibly diluted by unlabeled solvent $H_2{}^{16}O$. The magnitude of R_{H_2O} can be interpreted in terms of the rate constant of proton transfer from a donor group to the zinc-bound hydroxide according to the equation:

$$\frac{R_{H_2O}}{[E]} = \frac{k_B}{(1 + K_D/[H^+])(1 + [H^+]/K_A)} \quad (5)$$

where k_B is the maximal rate of proton transfer, K_D is the apparent acid dissociation constant for the donor group, and K_A is the apparent acid dissociation constant for the acceptor group (*19*). Experimental data for R_1 and R_{H_2O} were fit to modified versions of eqs 4 and 5 (see Results and Discussion

Table 1: Data Collection and Refinement Statistics for ECCA, HICA, and Their Bicarbonate Complexes[a]

	ECCA-HCO_3^- (PDB 2ESF)	HICA (PDB 2A8C)	HICA-HCO_3^- (PDB 2A8D)
Data Collection Statistics			
source	ALS BL-5.0.1	Rigaku RU-200	Rigaku RU-200
wavelength (Å)	1.0000	1.5418	1.5418
space group	$P4_322$	C_2	C_2
cell parameters (Å)	82.9, 162.2	232.7, 144.7, 52.4	232.8, 144.6, 52.1
cell parameters (deg)	90, 90, 90	90, 94.0, 90	90, 94.1, 90
resolution (Å)	54−2.25 (2.37−2.25)	25−2.30 (2.38−2.30)	30−2.20 (2.28−2.20)
no. of unique reflections	27655	65683	86683
redundancy	7.3 (7.3)	2.9	2.9
completeness (%)	99.9	85.7	99.6
R_{sym} (%)	8.0 (36.8)	4.5 (23.0)	4.3 (26.2)
$\langle I\rangle/\langle\sigma I\rangle$[b]	16.1 (3.7)	20.4 (3.04)	22.0 (3.18)
Refinement Statistics			
no. of unique reflections	27603	65633	86529
no. of reflections in test set	1351	3329	8684
R_{work} (%)	19.8	21.5	20.6
R_{free} (%)	22.8	25.9	24.0
no. of atoms			
protein	3430	10590	10590
ligand	8	30	54
ion	2	6	6
solvent	216	163	318
RMSD from ideal values[c]			
bond distance (Å)	0.006	0.0061	0.0056
bond angle (deg)	1.1	1.18	1.14
Ramachandran outliers (%)[d]	3.8	3.7	2.3

[a] Values in parentheses represent data for the highest resolution shell. [b] Reported as $\langle\langle I\rangle/\sigma\langle I\rangle\rangle$ in SCALA or SCALEPACK. [c] Ideal values from Engh and Huber (*42*). [d] Calculated using a strict boundary Ramachandran plot (*43*).

sections) using nonlinear least squares in Origin 6.0 (Microcal). Values of R_1/[E] and R_{H_2O}/[E] are reported here on a per subunit basis.

Crystallographic Methods. Rosettes of crystalline HICA were obtained in 48 h by the hanging drop method using 1.7 M $(NH_4)_2SO_4$, 4% (v/v) PEG-400, 0.10 M HEPES, pH 7.50, and 8−12 mg/mL protein at 4 °C. Individual crystals were separated using a probe and transferred to artificial mother liquor supplemented with 25% glycerol for 30 s, followed by flash cooling in liquid nitrogen. To prepare HICA complexed with bicarbonate ion, individual crystals were soaked for 15 min in artificial mother liquor containing 25% glycerol and 100 mM $NaHCO_3$. Data collection was performed with a rotating copper anode source (Rigaku RU-200) and an R-Axis IV image plate detector using 0.5° oscillations at a temperature of 95 K. Data were processed using DENZO and SCALEPACK (*20*) (HKL Research). An initial molecular replacement solution was obtained by using a modified ECCA (PDB entry 1I6P) search model using EPMR (*21*). This initial solution was subjected to rigid-body refinement, simulated annealing, and multiple rounds of refinement using CNS 1.1 (*22*) and model building in the program O (*23*).

Crystals of ECCA in space group $P4_322$ were grown as described previously (*12*) and transferred to 40% PEG-400 containing 250 mM $NaHCO_3$ and 100 mM MES at pH 7.0. After being soaked for 20 min, the crystals were flash frozen in liquid nitrogen and diffraction data collected at 115 K using beamline 5.0.1 of the Advanced Light Source, Lawrence Berkeley National Laboratories. The data, collected to 2.25 Å resolution, were indexed, reduced, and scaled using MOSFLM (*24*) and CCP4 (*25*). The previously determined structure for ECCA (PDB entry 1I6O), with all water molecules omitted, was used as a model. In this case, a molecular replacement search was unnecessary. An initial rigid-body refinement, using CNS 1.1 (*22*), reduced the *R* factor from 0.382 to 0.294 (R_{free} from 0.392 to 0.298). Phases calculated from the model were used in combination with experimental structure factor amplitudes to calculate electron density maps. The initial model was adjusted manually using the program O (*23*) to conform to $2F_o - F_c$ and $F_o - F_c$ difference Fourier maps. Simulated annealing omit maps were used in verifying the correctness of the model, and positional and *B*-factor refinement was performed prior to addition of bicarbonate and solvent molecules to the model. The final model was arrived at following multiple rounds of individual torsional and *B*-factor refinement using CNS (*22*) and addition of solvent molecules, combined with inspection and manual adjustment. Data collection and refinement statistics for all three models are reported in Table 1.

RESULTS

Overexpression and Purification of HICA. HICA was expressed in *E. coli* at levels of up to 40% of total protein, according to scanning densitometry of SDS−PAGE gels. One liter of overnight bacterial culture (≈25 g wet cell paste) typically yielded 10−20 mg of homogeneous enzyme. The molecular mass of purified HICA, determined from its elution volume during the last purification step on a calibrated size exclusion column (Superdex 200, Pharmacia), was 99 ± 14 kDa. This value is consistent with a molecular mass of 105.26 kDa calculated for a tetramer of HICA, including the zinc cofactor.

Overall Structure of HICA. The structure of HICA (PDB entry 2A8C) was determined by molecular replacement from data collected from a single crystal in the C_2 space group. Summary statistics are shown in Table 1. HICA has an overall fold and zinc coordination geometry that is essentially

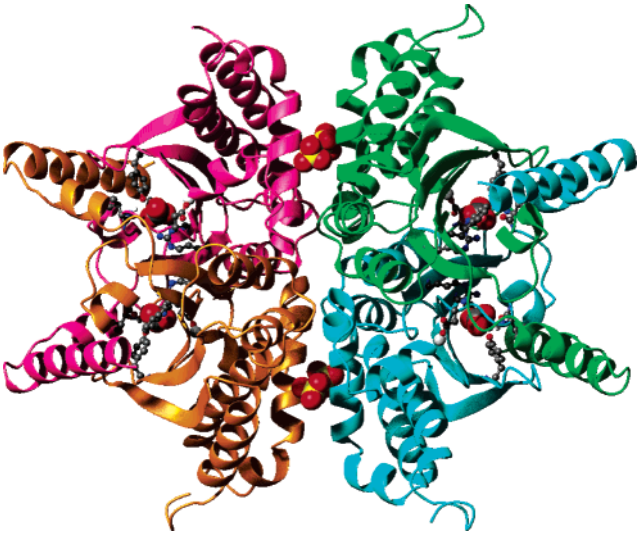

FIGURE 1: Ribbon diagram of the HICA native tetramer. Chains C−F of PDB entry 2A8C are depicted here in different colors. The active site zinc ions are depicted by light gray spheres; sulfate ions at the tetramerization interface are depicted as CPK models. This figure was prepared using the program MOLMOL (*39*).

identical to that of the ECCA structure determined previously (*11*). The C_α RMSD between ECCA and HICA for residues 35−200 is 0.804 Å. Each subunit adopts an α/β fold, with a central β-sheet composed mainly of four parallel strands (Figure 1). The zinc ion of each active site, located at the C-terminal edge of this sheet, is coordinated to four residues within the same monomer, Cys42, His98, Cys101, and Asp44, in an approximately tetrahedral geometry. The entire crystal structure shows that the native, biologically relevant tetramer is most likely a dimer of dimers.[2] Subunits related by a 2-fold symmetry axis (which lies along the central horizontal in the projection shown in Figure 1) constitute the fundamental dimer. This dimerization interface between subunits extends the β-sheet core and completes the formation of an active site pocket associated with the zinc ion bound by the opposing monomer. A second 2-fold axis (vertical in Figure 1) relates the two dimers of the native tetramer. The region between dimers, defined here as the tetramerization interface, contains four additional, strong electron density peaks $>5.0\sigma$, approximately spherical in shape. These symmetry-related regions of nonprotein density are surrounded by several basic residues: Arg160, Lys165, and Arg198 from one subunit, plus Arg124 from the neighboring subunit. This electron density has been interpreted as sulfate, which is present at high concentration in the crystallization conditions. The location of the sulfate binding sites in the biologically relevant unit is shown in Figure 1.

Noncatalytic Bicarbonate Binding Sites. Strong electron density in $F_o - F_c$ maps ($>3\sigma$) not explainable by protein or solvent is observed in ECCA and HICA crystals soaked in HCO_3^-. (PDB entries for these structures are 2ESF and 2A8D, respectively, with refinement statistics given in Table 1.) We have interpreted this electron density, triangular and planar in shape, as bicarbonate (Figure 2). The plane of the bicarbonate ion, located approximately 8 Å from the zinc ion, is roughly perpendicular to the local plane of the central β-sheet, nearest strand S1 (residues 37−43; see Figure 3). Two of the four zinc ligands, Cys42 and Asp44, are located near the C-terminal end of this strand, which is situated between strands S2 (residues 59−65) and S3 (residues 91−99). Strand S2 lies along the dimerization interface, and the two other zinc ligands, His98 and Cys101, occur at or just after the C-terminus of S3. The bicarbonate site is thus in the vicinity of both the active site and the dimerization interface and, relative to the zinc ion, is on the opposite side of the Asp44 ligand, the proposed site for the catalytic activation of substrate (*10*, *26*). The bicarbonate ion is surrounded by the side chains of Trp39, Arg64, and Tyr181. Each of these residues is in position to donate one or more hydrogen bonds to the bicarbonate ion. Main-chain groups do not play a significant role in direct interactions with bicarbonate, with the notable exception of the carbonyl oxygen of Val47, which is poised to act as a hydrogen bond acceptor. In addition to bicarbonate, this pocket contains two well-defined spherical peaks of electron density that we have

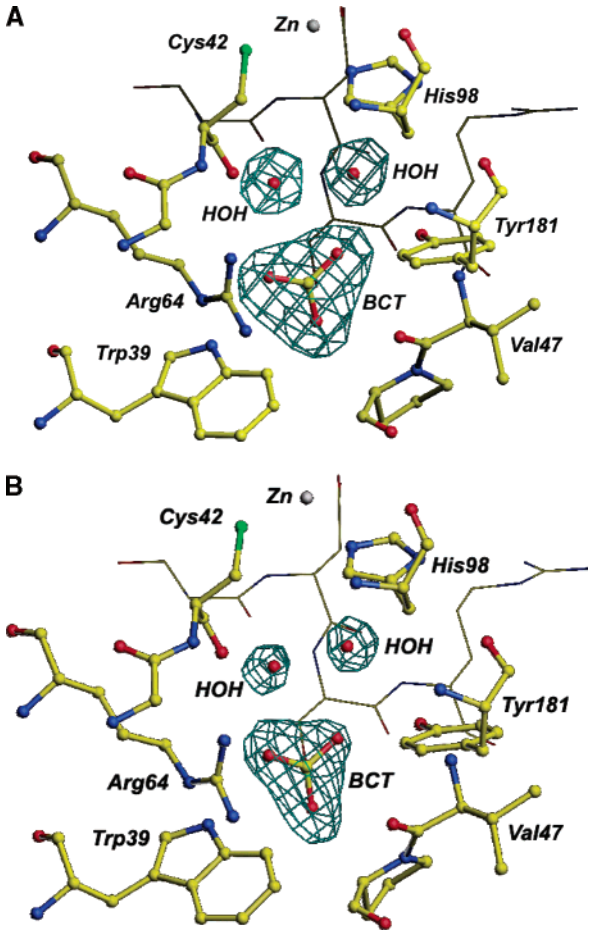

FIGURE 2: Noncatalytic bicarbonate binding sites in HICA (A) and ECCA (B). Fourier difference maps, shown in cyan at a contour of 3.5σ, were calculated as described in Experimental Procedures. In both cases, the final model in this vicinity is also shown, with some groups omitted for clarity. Key residues in the noncatalytic binding site are shown as ball-and-stick models. Thin lines denote the loop formed by residues 43−46. These figures were prepared using the program O (*23*) from PDB entries 2A8C and 2ESF, respectively.

[2] The asymmetric unit of the crystal, contained in PDB entry 2A8C, is comprised of six subunits, designated A−F. Of the three dimers per asymmetric unit, two dimers (chains C and E and chains D and F) constitute a biologically relevant unit, the native tetramer. A second tetramer straddles the C_2 axis in the unit cell and can be formed by applying crystallographic symmetry operators to chains A and B.

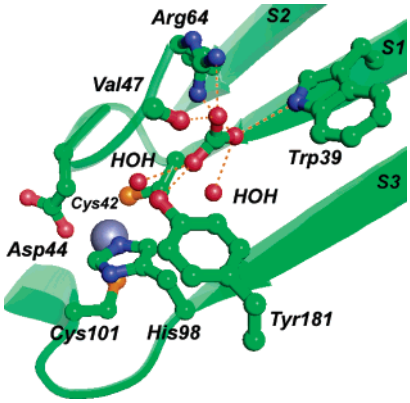

FIGURE 3: Detail of selected residues near the noncatalytic bicarbonate binding site of HICA. The zinc ion is represented by the white sphere. Also depicted are the four zinc ligands, Asp44, Cys42, His98, and Cys101. Likely hydrogen bonding interactions are denoted by orange dashed lines. This figure was prepared using the program PyMOL (*40*) for the HICA−bicarbonate complex (PDB entry 2A8D).

interpreted as water molecules. These waters are in position to form multiple hydrogen bonds with the oxygen atoms of the bicarbonate ion and protein functional groups. One of the water molecules is hydrogen-bonded to bicarbonate, the carbonyl oxygen of Cys96, and the main-chain amide of Cys42. This water, denoted henceforth as the common water, occurs in roughly the same location in most β-CA structures determined to date, including those from *P. sativum* (*7*) and *P. purpureum* (*10*). The second water molecule, the unique water, is also in a hydrogen bond with bicarbonate and is bound to the protein by the main-chain amides of Ser45 and Arg46, as well as the π-cloud of the imidazole ring of His98. Finally, a hydrogen bond between the main-chain amide of Val47 and the phenolic hydroxyl of Tyr181 further stabilizes the conformation of residues forming this pocket. The hydrogen-bonding network in the bicarbonate binding site is represented schematically in Figure 4.

Steady-State Kinetics. The pH profiles of k_{cat} and k_{cat}/K_m for the CO_2 hydration reaction at steady state for HICA (Figure 5) exhibit strong pH dependence, consistent with a requirement for the loss of multiple protons in order to generate the active, basic form of the enzyme. The pH dependence of k_{cat} (Figure 5A) can be adequately fit to a model, described by eq 6 , that requires the sequential loss

$$k_{obs} = \frac{k_{max}}{1 + [H^+]/K_{a2} + [H^+]^2/K_{a1}K_{a2}} \quad (6)$$

of two protons from two groups whose pK_a values are in this case not significantly different and near 8.3 in order to generate active enzyme. In eq 6, k_{obs} is the observed value of k_{cat} at any pH, k_{max} is the maximal value of k_{cat} at high pH, and K_{a1} and K_{a2} are acid dissociation constants corresponding to the stepwise ionization of the enzyme, $EH_2 \leftrightarrows EH^- + H^+ \leftrightarrows E^{2-} + 2\,H^+$, where the doubly deprotonated form is the active species. Values for these parameters are given in Figure 5. The k_{cat}/K_m data are consistent with a model, described by eq 7 (Figure 5B), that requires the

$$k_{obs} = \frac{k_{max}}{1 + [H^+]^4/K_a^4} \quad (7)$$

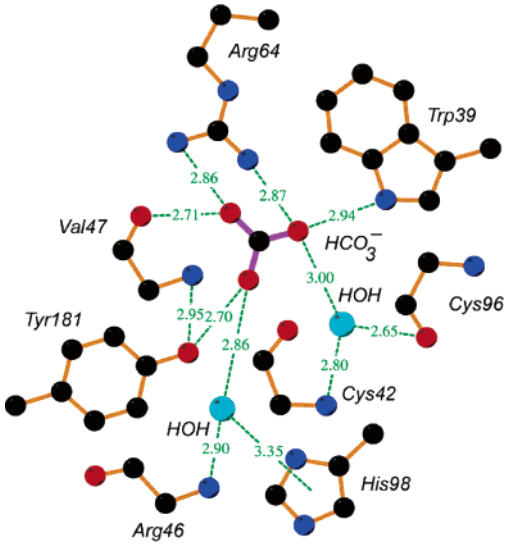

FIGURE 4: Schematic representation of the noncatalytic bicarbonate binding site. Main- and side-chain residues, as well as relevant solvent molecules in contact with the bicarbonate ion, are depicted. Dashed green lines and numbers represent inferred hydrogen-bonding interactions and the heavy atom−heavy atom distances, respectively. This figure was prepared using the program LIGPLOT (*41*) from the HICA−bicarbonate complex (PDB entry 2A8D).

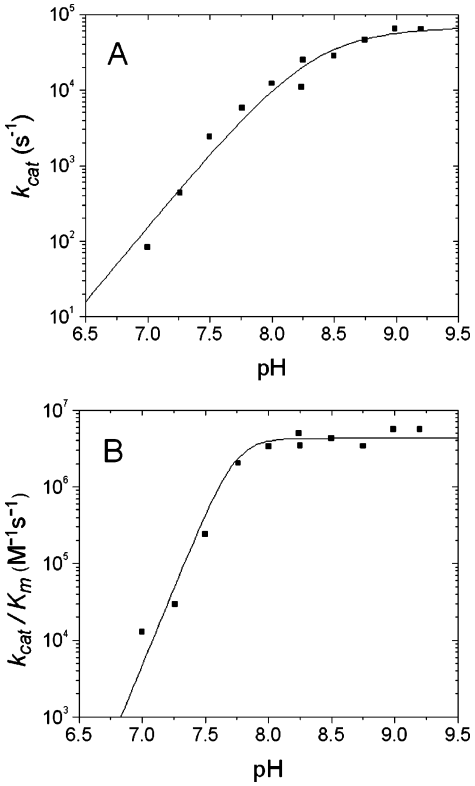

FIGURE 5: pH dependence of k_{cat} (A) and k_{cat}/K_m (B) for CO_2 hydration for HICA at steady state. Reaction conditions were 25 °C, 40 mM buffer (1-methylimidazole, pH 7.00−8.25; 1,2-dimethylimidazole, pH 8.25−9.25), 30−80 μM indicator dye (*p*-nitrophenol with 1-methylimidazole; *m*-cresol purple with 1,2-dimethylimidazole), 10 μM EDTA, 250 mM Na_2SO_4, and 0.4−15 μM enzyme. Kinetic parameters determined by least-squares fit to eq 6 (A) were $k_{max} = 69 \pm 29$ ms^{-1}, p$K_{a1} = 8.3 \pm 0.6$, and p$K_{a2} = 8.4 \pm 0.6$ or to eq 7 (B) were $k_{max} = 4.3 \pm 0.8$ μM^{-1} s^{-1} and p$K_a = 7.74 \pm 0.04$.

cooperative loss of four protons with a pK_a of 7.7 in order to generate the active enzyme. In eq 7, k_{obs} is the observed

value of k_{cat}/K_m at any pH, k_{max} is the maximal value of k_{cat}/K_m at high pH, and K_a is the acid dissociation constant of four identical groups that must be deprotonated, $EH_4 \leftrightarrows E^{4-} + 4H^+$, where the deprotonated species is the active form of the enzyme. Values for these parameters are given in the legend of Figure 5.

Oxygen-18 Exchange Kinetics. The pH profiles of R_1, R_{H_2O}, and k_{cat}/K_m (derived from ^{18}O exchange data) also show highly cooperative pH−rate profiles not consistent with simple one-proton ionizations. The pH dependence of R_1 can be fit to the equation:

$$\frac{R_1}{[E]} = \frac{k_{max}}{(1 + [H^+]^4/K_a^4)(1 + K_{Zn}^2/[H^+]^2)} \quad (8)$$

which shows a four-proton dependence at low pH and a two-proton dependence at high pH (Figure 6A). In eq 8, $R_1/[E]$ is the observed value of this rate constant at any pH, k_{max} is the maximal, intrinsic value of $R_1/[E]$, K_{Zn} is the acid dissociation constant of the zinc−water complex, and K_a is the acid dissociation constant of four groups that must be deprotonated, $EH_4 \leftrightarrows E^{4-} + 4H^+$, to form the active species of the enzyme. Values for all parameters are given in Figure 6. Equation 8 is similar to eq 7, except for the expected additional pH dependence on the ionization state of the active site zinc-bound water as required by eq 4 (*27*). The denominator term for the ionization of substrate CO_2/HCO_3^- in eq 4 is neither necessary nor observable for the pH range of data reported here, since pK_{CO_2} is approximately 6.3, and the data of Figure 6 is for pH values >7.5. For maximal $R_1/[E]$, eq 8 suggests that the active form of the enzyme has lost four protons cooperatively from a group or groups with a pK_a of 8.2, and two groups of pK_a 8.6, presumably Zn-OH_2, are protonated (Figure 6A). The pH dependence of R_{H_2O} is very similar in shape to that of R_1 (Figure 6B), again with a four-proton dependence at low pH and a two-proton dependence at high pH, suggesting that the most active form of the enzyme must cooperatively lose four protons for maximal activity. Equation 9 describes how these data might be best interpreted, with the high pH limb of the data originating from two donor groups that are capable of protonating the active site zinc hydroxide (*19*) as described in eq 5. Here k_{max} represents the maximal, intrinsic value of $R_{H_2O}/[E]$, and K_D represents the acid dissociation constant of groups that donate protons to Zn-OH_2 to enable loss of ^{18}O label to water (*27*). K_a has the same meaning as in eq 8. Values for all parameters in eq 9 are given in Figure 6. The

$$\frac{R_{H_2O}}{[E]} = \frac{k_{max}}{(1 + [H^+]^4/K_a^4)(1 + K_D^2/[H^+]^2)} \quad (9)$$

value of k_{cat}/K_m for the hydration reaction, calculated from ^{18}O exchange data (*27*), also fits well to a model described by eq 7 which requires the cooperative loss of four protons from groups with a pK_a of 8.3 to generate the active enzyme (Figure 6C).

HICA-catalyzed ^{18}O exchange appears to be strongly inhibited by HCO_3^-. Indeed, at pH values below 8.0, it is difficult to observe R_1 or R_{H_2O} at $CO_2 + HCO_3^-$ concentrations higher than 2 mM. At pH 8.75, where it is possible to accurately measure ^{18}O exchange kinetics over a range of

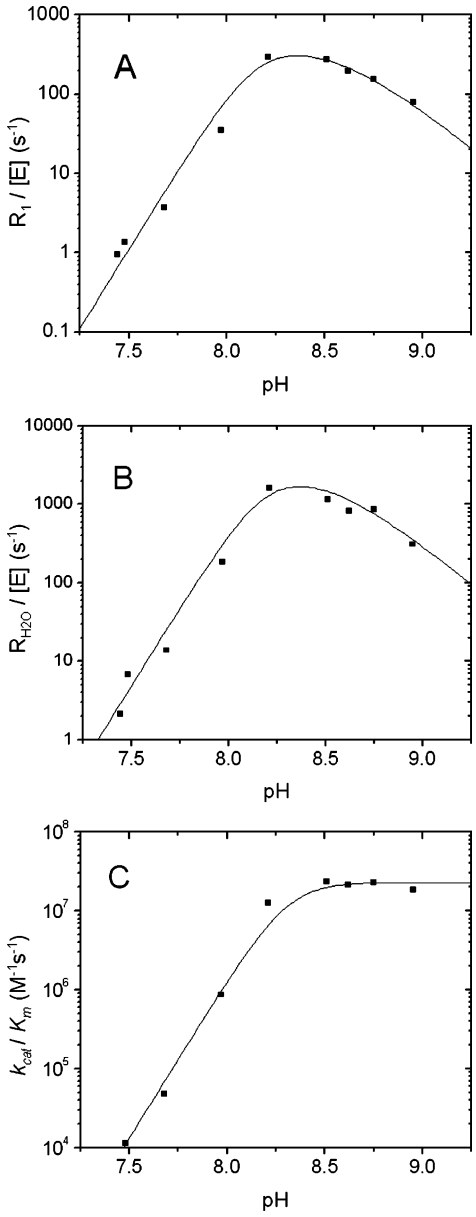

FIGURE 6: pH dependence of R_1 (A), R_{H_2O} (B), and k_{cat}/K_m for CO_2 hydration for HICA as determined by ^{18}O isotope exchange. Reaction conditions were 25 °C, 2 mM $CO_2 + HCO_3^-$, 10 μM EDTA, 250 mM Na_2SO_4, and 60−250 nM enzyme. Kinetic parameters determined by least-squares fit to eq 8 (A) were $k_{max} = 490 \pm 340$ s^{-1}, $pK_a = 8.2 \pm 0.1$, and $pK_{Zn} = 8.6 \pm 0.2$, to eq 9 (B) were $k_{max} = 3200 \pm 3700$ s^{-1}, $pK_a = 8.2 \pm 0.1$, $pK_D = 8.5 \pm 0.3$, or to eq 7 (C) were $k_{max} = 23 \pm 4$ μM^{-1} s^{-1} and $pK_a = 8.31 \pm 0.02$.

$CO_2 + HCO_3^-$ concentrations, the substrate dependence of both R_1 and R_{H_2O} is clearly biphasic. At low concentrations of $CO_2 + HCO_3^-$ these rates increase in a hyperbolic (Michaelis−Menten) fashion but at higher concentrations decrease in a cooperative fashion (Figure 7). These data can be adequately fit to a substrate inhibition model (see Discussion) in which HCO_3^- acts as both a substrate and an inhibitor:

$$k_{obs} = \frac{k_{max}[S]}{(K_{eff} + [S])(1 + [S]^2/K_i^2)} \quad (10)$$

In eq 10, k_{obs} is the observed value of $R_1/[E]$ or $R_{H_2O}/[E]$,

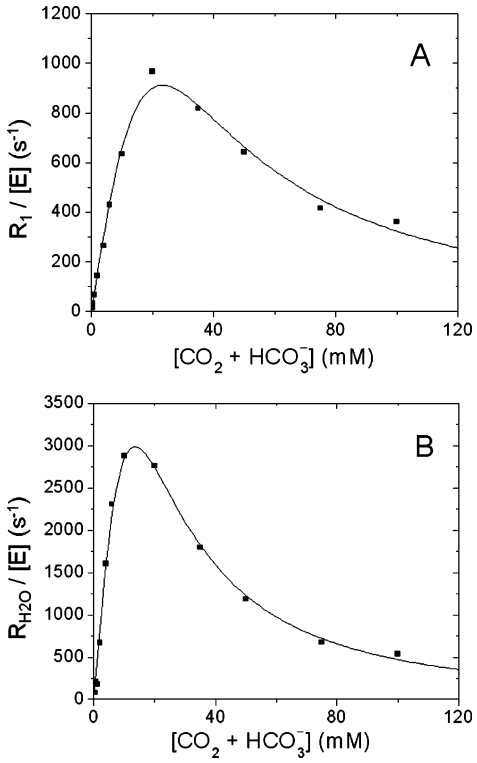

FIGURE 7: Substrate dependence of R_1 (A) and R_{H_2O} (B) for HICA. Reaction conditions were 25 °C, pH 8.75, 10 μM EDTA, 250 mM Na_2SO_4, and 60−250 nM enzyme. Kinetic parameters determined by least-squares fit to eq 10 were (A) $k_{max} = 14 \pm 11$ ms^{-1}, $K_{eff} = 170 \pm 140$ mM, and $K_i = 26 \pm 3$ mM and (B) $k_{max} = 34 \pm 24$ ms^{-1}, $K_{eff} = 75 \pm 55$ mM, and $K_i = 16 \pm 2$ mM.

[S] is the combined concentration of $CO_2 + HCO_3^-$, k_{max} is the maximal intrinsic value of these rate constants, K_{eff} is the concentration of $CO_2 + HCO_3^-$ that yields half-maximal R/[E], and K_i is the effective inhibitor dissociation constant based on the concentration of $CO_2 + HCO_3^-$ present.

DISCUSSION

The structure of uncomplexed HICA reported here is remarkably similar to that of uncomplexed ECCA and the other *P. purpureum*-like β-CAs and represents the fourth structure of this class, with Asp44 in lieu of water as the fourth zinc ligand. The observation of this β-CA structure for enzymes from four different organisms suggests that these structures are not crystallization artifacts or anomalous structures but are instead likely to be physiologically relevant. Likewise, the novel bicarbonate binding mode identified is common to both the HICA and ECCA structures and unlikely to be artifactual. The site of bicarbonate binding is quite distinct from the zinc coordination site at which the dehydration of bicarbonate as a substrate is expected to occur.

This latter observation may be important in an explanation for the existence of two distinct coordination states in β-CA structures. It has been previously suggested that the *P. purpureum*-like β-CA structures represent inactive conformations of the enzyme (*11*) and that the equivalent of Asp44 in HICA might be a mobile, exchangeable zinc ligand (*10*). Building upon these suggestions, if bicarbonate binding were only compatible with an inactive conformation of the enzyme, it raises the possibility that a given type of β-CA adopts either of these two distinct conformations depending on bicarbonate levels. In other words, with respect to certain β-CAs, bicarbonate acts as a regulator as well as a substrate. While bicarbonate is of course a ubiquitous metabolite and physiological buffer, catalytic and regulatory roles for it have been characterized. Bicarbonate stimulates the activity of soluble adenylyl cyclase (sAC), an evolutionarily conserved class of adenylyl cyclases that act at an upstream position in various intracellular signaling pathways (*28*). Bicarbonate has also been shown to act catalytically as a general base in dizinc leucine aminopeptidase (*29*).

The noncatalytic bicarbonate binding site in HICA and ECCA seems to be exquisitely designed for recognition of this ion. The side chains of Trp39, Arg64, and Tyr181, as well as two water molecules, donate no less than six hydrogen bonds to the negatively charged bicarbonate ion, and a lone, critical hydrogen bond acceptor interaction with the carbonyl of Val47 assists in discrimination between HCO_3^- and other competing anions that cannot act as a hydrogen bond donor. By virtue of the second hydrogen bond contributed by its main-chain amide, to Tyr181 OH, Val47 also participates in the formation of the bicarbonate binding pocket by pinning down the critical 44−47 loop.

Two questions arise in light of these observations: How do other examples of bicarbonate reported in protein structures compare with the noncatalytic binding site in HICA and ECCA, and what role, if any, does the ligand play in the function of proteins in which it has been observed? A survey of protein structures containing bicarbonate reveals that, in general, proximity to an arginine side chain and ligation to metal ions are the most common structural features. Of the cases examined, the one that most resembles the present case is found in the structure of cystathionine β-lyase from *E. coli*, where bicarbonate is bound tightly near the pyridoxal phosphate cofactor (*30*). The same side chains participate in HCO_3^- binding as in the β-CA site, but the sites are stereochemically distinct and do not appear to be homologous. The conserved arginine acts as a carboxylate recognition motif for the enzyme's normal substrate, and bicarbonate apparently binds as a competitive inhibitor. In the case of sAC, where bicarbonate has been inferred to cause a presumably allosteric activation by promoting conformational changes at the active site and recruitment of a second catalytic metal ion, the location of its action has remained undefined (*31*). Thus, the noncatalytic binding site in HICA and ECCA appears to be novel.

The biphasic, substrate inhibition kinetics of R_1 and R_{H_2O} in HICA is not observed in other classes of CAs, nor in *Arabidopsis thaliana* β-CA (*18*). In addition, the highly cooperative pH−rate profiles for k_{cat}, k_{cat}/K_m, R_1, and R_{H_2O} are not observed for other CAs. Indeed, to date no carbonic anhydrase has been observed to have cooperative kinetics, not the dimeric β-CA from *M. thermoautotrophicum* (*32*), the trimeric γ-CA from *Methanosarcina thermophila* (*33*), nor the octameric plant β-CAs from *A. thaliana* (*18*) and *P. sativum* (*34*). It is perhaps significant that the plant β-CAs, as well as the β-CA from *M. thermoautotrophicum*, are missing key elements of the noncatalytic bicarbonate binding site described here for ECCA and HICA. In particular, in both *P. sativum* and *A. thaliana* β-CA, the equivalent of Trp39 in HICA is replaced by a valine residue. In the *M. thermoautotrophicum* enzyme, the equivalents of both Trp39 and Tyr181 in HICA are replaced by isoleucine, and the equivalent of Arg64 in HICA is replaced by lysine. Another

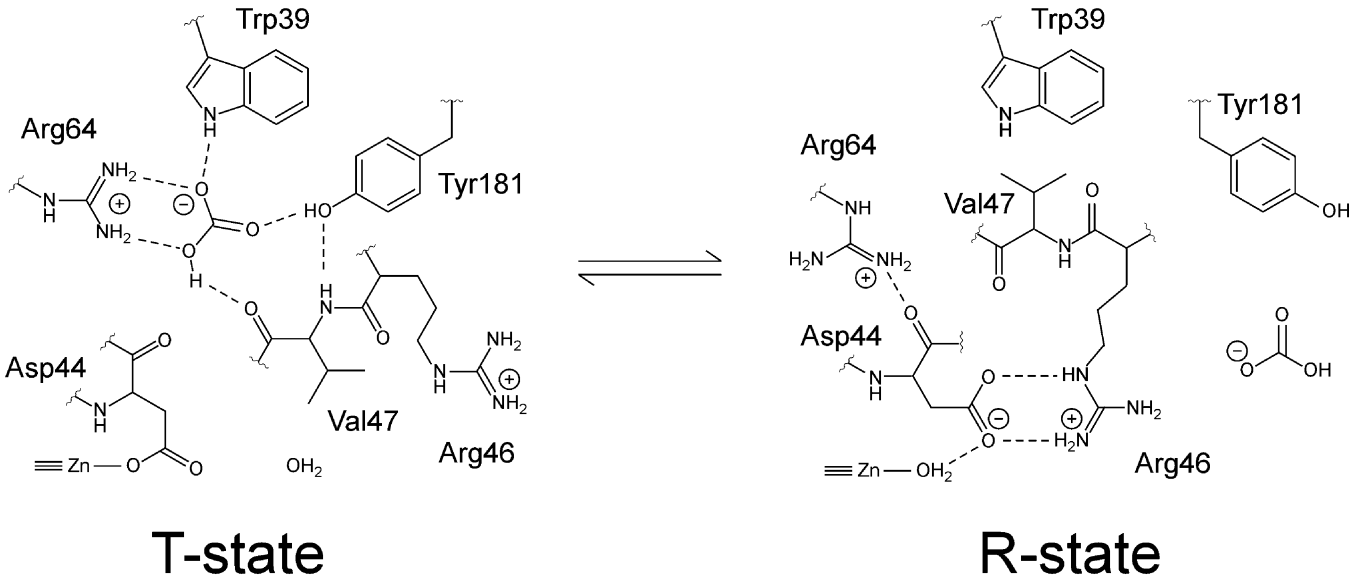

FIGURE 8: Schematic of key active site and noncatalytic bicarbonate binding site interactions in the proposed active and inactive conformations of HICA.

difference of note concerns the S1 residue immediately preceding the first zinc ligand, which is Gly41 in HICA and ECCA. The corresponding residue is also glycine in the *P. pupureum* and *M. tuberculosis* Rv3588c β-CAs, while a non-glycine residue occupies this position in the plant, *M. thermoautotrophicum*, as well as the *M. tuberculosis* Rv1284 β-CAs. The absence of a β-carbon in this location creates space adjacent to the β-sheet that may be a steric necessity for accommodation of bicarbonate. While the sampling of β-CAs whose kinetics have been thoroughly investigated is admittedly small, nonetheless we note that β-CAs that are missing the key features of the noncatalytic bicarbonate binding site observed in HICA and ECCA do not exhibit cooperative kinetics.

Given the proximity of the noncatalytic bicarbonate binding site to the catalytically important zinc ion, it is reasonable to suspect that this site might in some way influence the catalytic activity of the enzyme. In a two-state model for cooperative kinetics (*35*), the class of β-CA structures typified by the coordination of Asp44 as a fourth ligand to the catalytically important zinc ion provides an attractive model for an inactive conformation of β-CA. The possibility that certain β-CAs might adopt an alternative, inactive conformation in which Asp44 displaces the catalytically essential water molecule has been suggested previously (*11*), where the *P. sativum* CA structure served as a model for the as yet unobserved active conformation of ECCA. A comparison of structures, discussed further below, in light of the noncatalytic bicarbonate binding site identified in HICA and ECCA, indicates that adoption of a *P. sativum*-like structure by HICA or ECCA would disrupt the bicarbonate binding pocket. Strictly speaking, the inactive conformation could exist in the absence of allosteric bicarbonate binding. However, the existence of an active conformation with bicarbonate bound in this site appears to be highly unlikely due to structural constraints. For the purposes of this discussion, we will consider there to be two principally populated states, with the *P. purpureum*-like β-CA structure observed in HICA/ECCA serving as a model for an inactive "T-state" that is stabilized by bicarbonate and the *P. sativum* CA structure (PDB entry 1EKJ) as providing the key elements of an "R-state" model. This scheme is illustrated in Figure 8.

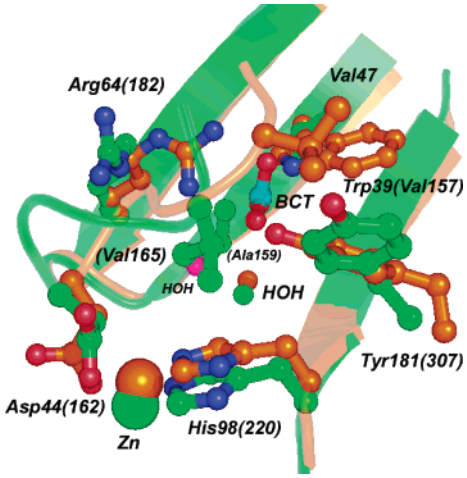

FIGURE 9: Structure alignment of HICA (PDB entry 2A8D) and PSCA (PDB entry 1EKJ). HICA and PSCA ribbons, carbon atoms, zinc ions, and common water molecules are colored orange and green, respectively. The unique water molecule in HICA is colored magenta. Structures were aligned and rendered using PyMOL (*40*). Residue numbers are for HICA (no parentheses) or PSCA (parentheses).

In *P. sativum* CA, Asp44 is displaced by a water molecule, but remains as a hydrogen bond acceptor from the zinc-bound water, and is engaged in a salt bridge with Arg46.[3] The conformation of the loop from residues 44−47, which includes important elements of the bicarbonate binding site, is radically different. The position of theVal47 side chain would overlap that of the unique water molecule (Figure 9). While the exact nature of the coupling between bicarbonate binding in the noncatalytic site and the equilibrium between the proposed active and inactive states is unknown, it is quite plausible that the binding of bicarbonate ion could exert and have influence on the coordination state of the zinc ion. We

[3] All residue numbers in this part of the Discussion are numbered as the equivalent residue in HICA.

note that the bicarbonate ion and the water molecules that are directly associated with it interact with residues in or around the zinc-ligation sphere. For example, the water molecules bound to the bicarbonate interact with the zinc ligands His98 and Cys42 and also with the main chain of Arg46, which is predicted by the scheme represented in Figure 8 to interact with Asp44 in the active conformation. Bicarbonate ion and its ligand Tyr181 both interact with the main chain of Val47, which anchors the 44−47 loop over the bicarbonate binding site. The loss of bicarbonate from this site might lead to a reorganization of this loop that allows the carboxylate group of Asp44 to pair with Arg46 instead of ligating zinc. Additionally, in *P. sativum* CA, the structural region corresponding to the noncatalytic bicarbonate binding pocket in HICA has collapsed to form a hydrophobic region surrounding the side chain of Val47, which occupies the approximate position of the bicarbonate ion in HICA. In *P. sativum* CA the insertion of the Val47 side chain into the hydrophobic pocket comprised by Phe309, Ile218, and Ala159 significantly reorients the loop corresponding to residues 44−47 in HICA that contain the catalytically important Arg46 residue. Site-directed mutagenesis of the *M. thermoautotrophicum* enzyme suggests that the coordination of Arg36 (equivalent to Arg46 in HICA) is essential for orienting Asp44 to generate the active species of enzyme (*8*). Therefore, it seems likely that the side chain of Val47 could provide the mechanism to couple an inactive−active state conformational equilibrium to bicarbonate ion. That is, the binding of bicarbonate stabilizes the inactive state by preventing the rotation of the 44−47 loop required to insert the side chain of Val47 into the bicarbonate binding site which would thereupon allow the coordination of Asp44 and Arg46 to generate active enzyme with a zinc-bound water molecule. The bicarbonate-binding residue Arg64 has an apparently quite distinct role in the context of the *P. sativum* CA structure. The Arg64 guanidinium group forms three different hydrogen bonds to the main-chain carbonyl oxygens of residues Cys42 and Asp44, providing structural stability to this particular local main-chain conformation (*36*), which here is characteristic of an active β-CA. Loss of this stabilization would be concomitant with the redirection of the Arg64 guanidinium group to interaction with bicarbonate, as seen in HICA/ECCA, facilitating adoption of a main-chain conformation of residues 44−47 characteristic of an inactive β-CA. The envisioned transition between states would be expected to occur in a concerted fashion, with changes involving Arg64 acting synergistically with the other changes discussed above.

Furthermore, since both the active site zinc and the bicarbonate binding site lie at or near the dimerization interface, binding of bicarbonate ion in one subunit could also affect neighboring subunits. Indeed, the noncatalytic bicarbonate binding sites are only 15 Å apart in the principal HICA dimer (Figure 10). Arg64, located on β-strand S2, is the bicarbonate-binding residue that lies closest to the neighboring subunit across the dimerization interface. In HICA, there are intersubunit hydrogen bonds between His63NHδ−Arg64O, Arg64O−Arg64NH, S43OHγ−Val62O, and Arg46NH−Asn33O. The corresponding residues in *P. sativum* carbonic anhydrase are not involved in intersubunit contacts.

FIGURE 10: Cartoon diagram of a single dimer of HICA (PDB entry 2A8D). Individual monomer chains are colored blue and orange. Each monomer depicts the noncatalytic bicarbonate binding site, including bicarbonate ion (red and gray spheres), principal interacting side chains Trp39, Arg64, and Tyr181 (sticks), and the active site zinc ion (magenta spheres). A short helical segment (residues 48−54) has been rendered invisible for clarity. This figure was prepared using PyMOL (*40*).

While the structural data suggest that bicarbonate serves a likely regulatory role in HICA, the kinetics data additionally suggest that this role is allosteric in nature. The sharp pH-dependent transition from inactive to active protein around pH 8 is seen in kinetics measurements of both CO_2 hydration (Figures 5B and 6C) and HCO_3^- dehydration (Figure 6A,B). That all of these pH dependences have the same directionality for both the forward and reverse reactions, that is, the enzyme is most active at high pH for both hydration and dehydration reactions, indicates that the relevant proton ionizations are not integral to the catalytic mechanism, else the pH profiles for CO_2 hydration and HCO_3^- dehydration would be inverse of each other. Rather, the steep pH dependence of k_{cat}/K_m, R_1, or R_{H_2O} at lower pH values in Figures 5B and 6 must instead relate to processes which affect the fraction of active enzyme available, e.g., a pH-dependent equilibrium between active and inactive conformations.

The simplest explanation for the pH−rate profiles of k_{cat}/K_m, R_1, and R_{H_2O} (Figures 5B and 6) at lower pH values is a cooperative transition of the biologically relevant tetramer between an inactive conformation at low pH to an active conformation at high pH, in which all four subunits act in a concerted fashion: $(EH)_4 \leftrightarrows (E^-)_4 + 4H^+$. The most plausible ionization event that triggers this conformation change is that of the zinc-bound water molecule. At high pH, when the zinc-bound water has ionized to hydroxide, Asp44 is displaced from the active site and instead ion pairs with Arg46 in a manner similar to that seen in *P. sativum* β-CA; at low pH, protonation of the zinc-bound hydroxide to the more labile zinc-bound water allows its facile displacement by Asp44, leading to a catalytically impotent form of the enzyme. Furthermore, HCO_3^- additionally stabilizes the

inactive state, with Asp44 ligated to the active site zinc, by binding to its noncatalytic pocket. This hypothesis is consistent with the profound bicarbonate inhibition of R_1 and R_{H_2O} at chemical equilibrium, especially at low pH.

An alternative explanation of the low-pH limb of the data of Figures 5B and 6 is that the principal allosteric unit is a dimer. In this model the cooperative low-pH transition of the pH−rate profiles of k_{cat}/K_m, R_1, and R_{H_2O} (Figures 5B and 6) would necessarily be interpreted in terms of two successive two-proton ionizations: $(EH_2)_2 \leftrightarrows (EH^-)_2 + 2H^+ \leftrightarrows (E^{2-})_2 + 4H^+$. In this case the term $1 + [H^+]^4/K_a^4$ in eqs 7−9 is replaced by the term $1 + [H^+]^2/K_{a2}^2 + [H^+]^4/K_{a1}^2K_{a2}^2$. The latter term reduces to the former if $K_{a2} \ll K_{a1}$ (i.e., the pK_a values are "crossed") and the product $K_{a1} \times K_{a2}$ in the latter is equal to K_a in the former. Crossing the pK_a values by as little as 0.5 pH unit from each other is sufficient to render these two models kinetically indistinguishable. While these two potential models cannot be distinguished kinetically, they do place some constraints on the interpretation of the pH−rate data. In the present case, if the allosteric unit is indeed a dimer rather than a tetramer, then there must be two ionizable groups in each monomer, both of which must be deprotonated to trigger the transition from inactive to inactive conformation. A possible scenario is that the deprotonation of the zinc-bound water (pK_{a2}) triggers a structural change in the dimer that allows a second, unidentified residue with a lower pK_a (pK_{a1}) to deprotonate in each subunit of the dimer. In this scenario, the true pK_a of the zinc-bound water would be higher and the pK_a of the unidentified residue lower than the kinetically determined pK_a using eqs 7−9.

Several additional lines of evidence strengthen the hypothesis that the allosteric unit of HICA is a dimer. First, the high-pH limb of the pH−rate profiles of R_1 clearly shows a two-proton dependence. That is, two groups must be cooperatively protonated to generate the active species of the enzyme. Because the high-pH limb of R_1 (Figure 6A) tracks the ionization state of the zinc-bound water (*27*), this suggests that an active enzyme species for HCO_3^- dehydration can be formed by the protonation of only two, and not four, of the zinc hydroxides in the biologically relevant unit of HICA. Similarly, the high-pH limb of R_{H_2O} (Figure 6B) suggests that only two proton transfer donors (*17*) need be protonated to generate an active species for proton transfer in the HCO_3^- dehydration reaction. Third, the HCO_3^- inhibition of R_1 and R_{H_2O} at chemical equilibrium (Figure 7) can be satisfactorily modeled only if it is assumed that the inhibited species binds noncompetitively to two molecules of bicarbonate, e.g., $(E)_2 + 2HCO_3^- \leftrightarrows (E{-}HCO_3^-)_2$, where E_2 is the catalytically active species. This model predicts inhibition behavior as described by eq 10 and fits the data in Figure 7 very well. Finally, the structures of HICA and ECCA both have one tight and one loose interface between monomers, the former corresponding to the dimerization interface and the latter to the tetramerization interface. This suggests that intersubunit communication is more likely within the tightly bound dimer. The tight dimerization interface is where the catalytic and noncatalytic sites are located, and Arg64, which is located on this interface, is a likely candidate for mediating intersubunit communication.

The structural and kinetic data presented here provide a strong case that HICA and ECCA can adopt two alternative conformations and that bicarbonate ion binding to a noncatalytic site stabilizes the inactive conformation. Although neither HICA nor ECCA have been crystallized in an alternative conformation to those reported here, the kinetic evidence here strongly suggests that it must adopt an alternative conformation in a highly cooperative fashion. The principal structural features seen in the noncatalytic HCO_3^- binding site for HICA and ECCA are shared with other members of the β-CA class, suggesting that there are other members of this class that may also exhibit cooperative kinetics, including the CAs from *P. purpureum* and *M. tuberculosis* Rv3588c. The physiological role for the allosteric regulation of certain β-CAs is not clear, but it has been shown that ECCA (*37*) and a β-CA from yeast (*38*) are essential for aerobic growth of these organisms, and it has been suggested that CA may be necessary to provide HCO_3^- for lipid biosynthesis. One might speculate that the allosteric regulation of β-CAs is used to maintain a critical concentration of HCO_3^- for biosynthesis during periods of high growth rates.

ACKNOWLEDGMENT

X-ray diffraction data for PDB entries 2A8C and 2A8D were collected at the National Institute for Diabetes, Digestive, and Kidney Disease, National Institutes of Health, Bethesda, MD. R.S.R. is indebted to David Davies, for allowing the use of the facility, and to Fred Dyda, Jessica Bell, and Thang Chiu, for advice and many helpful discussions.

REFERENCES

1. Hewett-Emmett, D. (2000) Evolution and distribution of the carbonic anhydrase gene families, *EXS 90*, 29−76.
2. Alber, B. E., and Ferry, J. G. (1994) A carbonic anhydrase from the archaeon *Methanosarcina thermophila*, *Proc. Natl. Acad. Sci. U.S.A. 91*, 6909−6913.
3. Roberts, S. B., Lane, T. W., and Morel, F. M. M. (1997) Carbonic anhydrase in the marine diatom *Thalassiosira weissflogii* (Bacillariophyceae), *J. Phycol. 33*, 845−850.
4. Lane, T. W., Saito, M. A., George, G. N., Pickering, I. J., Prince, R. C., and Morel, F. M. M. (2005) A cadmium enzyme from a marine diatom, *Nature 435*, 42.
5. So, A. K., Espie, G. S., Williams, E. B., Shively, J. M., Heinhorst, S., and Cannon, G. C. (2004) A novel evolutionary lineage of carbonic anhydrase (epsilon class) is a component of the carboxysome shell, *J. Bacteriol. 186*, 623−630.
6. Smith, K. S., Jakubzick, C., Whittam, T. S., and Ferry, J. G. (1999) Carbonic anhydrase is an ancient enzyme widespread in prokaryotes, *Proc. Natl. Acad. Sci. U.S.A. 96*, 15184−15189.
7. Kimber, M. S., and Pai, E. F. (2000) The active site architecture of *Pisum sativum* β-carbonic anhydrase is a mirror image of that of α-carbonic anhydrases, *EMBO J. 19*, 1407−1418.
8. Strop, P., Smith, K. S., Iverson, T. M., Ferry, J. G., and Rees, D. C. (2001) Crystal structure of the "cab"-type beta class carbonic anhydrase from the archaeon *Methanobacterium thermoautotrophicum*, *J. Biol. Chem. 276*, 10299−10305.
9. Suarez Covarrubias, A., Larsson, A. M., Hogbom, M., Lindberg, J., Bergfors, T., Bjorkelid, C., Mowbray, S. L., Unge, T., and Jones, T. A. (2005) Structure and function of carbonic anhydrases from *Mycobacterium tuberculosis*, *J. Biol. Chem. 280*, 18782−18789.
10. Mitsuhashi, S., Mizushima, T., Yamashita, E., Yamamoto, M., Kumasaka, T., Moriyama, H., Ueki, T., Miyachi, S., and Tsukihara, T. (2000) X-ray structure of β-carbonic anhydrase from the red alga, *Porphyridium purpureum*, reveals a novel catalytic site for CO_2 hydration, *J. Biol. Chem. 275*, 5521−5526.
11. Cronk, J. D., Endrizzi, J. A., Cronk, M. R., O'Neill J, W., and Zhang, K. Y. (2001) Crystal structure of *E.* coli beta-carbonic

anhydrase, an enzyme with an unusual pH-dependent activity, *Protein Sci. 10*, 911−922.
12. Cronk, J. D., O'Neill, J. W., Cronk, M. R., Endrizzi, J. A., and Zhang, K. Y. J. (2000) Cloning, crystallization and preliminary characterization of a β-carbonic anhydrase from *Escherichia coli*, *Acta Crystallogr. D 56*, 1176−1179.
13. Khalifah, R. G. (1971) Carbon dioxide hydration activity of carbonic anhydrase. I. Stop-flow kinetic studies on the native human isoenzymes B and C, *J. Biol. Chem. 246*, 2561−2573.
14. Pocker, Y., and Bjorkquist, D. W. (1977) Comparative studies of bovine carbonic anhydrase in water and water-d_2. Stopped-flow studies of the kinetics of interconversion of carbon dioxide and bicarbonate(1−) ion, *Biochemistry 16*, 5698−5707.
15. Ghannam, A. F., Tsen, W., and Rowlett, R. S. (1986) Activation parameters for the carbonic anhydrase II-catalyzed hydration of carbon dioxide, *J. Biol. Chem. 261*, 1164−1169.
16. Rowlett, R. S., Gargiulo, N. J., III, Santoli, F. A., Jackson, J. M., and Corbett, A. H. (1991) Activation and inhibition of bovine carbonic anhydrase III by dianions, *J. Biol. Chem. 266*, 933−941.
17. Silverman, D. N. (1982) Carbonic anhydrase: Oxygen-18 exchange catalyzed by an enzyme with rate-contributing proton-transfer steps, *Methods Enzymol. 87*, 732−752.
18. Rowlett, R. S., Tu, C., McKay, M. M., Preiss, J. R., Loomis, R. J., Hicks, K. A., Marchione, R. J., Strong, J. A., Donovan, G. S., Jr., and Chamberlin, J. E. (2002) Kinetic characterization of wild-type and proton transfer-impaired variants of beta-carbonic anhydrase from *Arabidopsis thaliana*, *Arch. Biochem. Biophys. 404*, 197−209.
19. Silverman, D. N., Tu, C., Chen, X., Tanhauser, S. M., Kresge, A. J., and Laipis, P. J. (1993) Rate-equilibria relationships in intramolecular proton transfer in human carbonic anhydrase III, *Biochemistry 32*, 10757−10762.
20. Otwinowski, Z., and Minor, M. (1997) Processing of X-ray diffraction data collected in oscillation mode, *Methods Enzymol. 276*, 307−326.
21. Kissinger, C. R., Gehlhaar, D. K., and Fogel, D. B. (1999) Rapid automated molecular replacement by evolutionary search, *Acta Crystallogr. D 55*, 484−491.
22. Brünger, A. T., Adams, P. D., Clore, G. M., DeLano, W. L., Gros, P., Grosse-Kunstleve, R. W., Jiang, J.-S., Kuszewski, J., Nilges, M., Pannu, N. S., et al. (1998) Crystallography and NMR system: A new software suite for macromolecular structure determination, *Acta Crystallogr. D 54*, 905−921.
23. Jones, T. A., Zou, J.-Y., Cowan, S. W., and Kjeldgaard, M. (1991) Improved methods for building protein models in electron density maps and the location of errors in these models, *Acta Crystallogr. A 47*, 110−119.
24. Leslie, A. G. W. (1992) Recent changes to the MOSFLM package for processing film and image data, *Joint CCP4 and ESF-EACMB Newsletter on Protein Crystallography*.
25. CCP4 (Collaborative Computational Project No. 4) (1994) The CCP4 suite: Programs for protein crystallography, *Acta Crystallogr. D 50*, 760−763.
26. Kimber, M. S., Coleman, J. R., and Pai, E. F. (2000) β-carbonic anhydrase from *Pisum sativum*: crystallization and preliminary x-ray analysis, *Acta Crystallogr. D 56*, 927−929.
27. Silverman, D. N. (1973) Kinetics and detection of carbonic anhydrase by oxygen-18 exchange techniques, *Proc. Int. Conf. Stable Isot. Chem., Biol., Med., 1st*, 239−245.
28. Kobayashi, M., Buck, J., and Levin, L. R. (2004) Conservation of functional domain structure in bicarbonate-regulated "soluble" adenylyl cyclases in bacteria and eukaryotes, *Dev. Genes Evol. 214*, 503−509.
29. Sträter, N., Sun, L., Kantrowitz, E. R., and Lipscomb, W. N. (1999) A bicarbonate ion as a general base in the mechanism of peptide hydrolysis by dizinc leucine aminopeptidase, *Proc. Natl. Acad. Sci. U.S.A. 96*, 11151−11155.
30. Clausen, T., Huber, R., Laber, B., Pohlenz, H. D., and Messerschmidt, A. (1996) Crystal structure of the pyridoxal-5′-phosphate dependent cystathionine beta-lyase from *Escherichia coli* at 1.83 Å, *J. Mol. Biol. 262*, 202−224.
31. Steegborn, C., Litvin, T. N., Levin, L. R., Buck, J., and Wu, H. (2005) Bicarbonate activation of adenylyl cyclase via promotion of catalytic active site closure and metal recruitment, *Nat. Struct. Mol. Biol. 12*, 32−37.
32. Smith, K. S., Ingram-Smith, C., and Ferry, J. G. (2002) Roles of the conserved aspartate and arginine in the catalytic mechanism of an archaeal beta-class carbonic anhydrase, *J. Bacteriol. 184*, 4240−4245.
33. Alber, B. E., Colangelo, C. M., Dong, J., Staalhandske, C. M. V., Baird, T. T., Tu, C., Fierke, C. A., Silverman, D. N., Scott, R. A., and Ferry, J. G. (1999) Kinetic and spectroscopic characterization of the gamma-carbonic anhydrase from the methanoarchaeon *Methanosarcina thermophila*, *Biochemistry 38*, 13119−13128.
34. Johansson, I. M., and Forsman, C. (1993) Kinetic studies of pea carbonic anhydrase, *Eur. J. Biochem. 218*, 439−446.
35. Monod, J., Wyman, J., and Changeux, J.-P. (1965) On the nature of allosteric transitions: a plausible model, *J. Mol. Biol. 12*, 88−118.
36. Borders, C. L. J., Broadwater, J. A., Bekeny, P. A., Salmon, J. E., Lee, A. S., Eldridge, A. M., and Pett, V. B. (1994) A structural role for arginine in proteins: multiple hydrogen bonds to backbone carbonyl oxygens, *Protein Sci. 3*, 541−548.
37. Merlin, C., Masters, M., McAteer, S., and Coulson, A. (2003) Why is carbonic anhydrase essential to *Escherichia coli*?, *J. Bacteriol. 185*, 6415−6424.
38. Clark, D., Rowlett, R. S., Coleman, J. R., and Klessig, D. F. (2004) Complementation of the yeast deletion mutant ΔNCE103 by members of the beta class of carbonic anhydrases is dependent on carbonic anhydrase activity rather than on antioxidant activity, *Biochem. J. 379*, 609−615.
39. Engh, R. A., and Huber, R. (1991) Accurate bond and angle parameters for X-ray protein structure refinement, *Acta Crystallogr. A 47*, 392−400.
40. Kleywegt, G. J. (2000) Validation of protein crystal structures, *Acta Crystallogr. D 56*, 249−265.
41. Koradi, R., Billeter, M., and Wuthrich, K. (1996) MOLMOL: a program for display and analysis of macromolecular structures, *J. Mol. Graphics 14*, 51−55, 29−32.
42. Wallace, A., Laskowski, R., and Thornton, J. (1995) LIGPLOT: A program to generate schematic diagrams of protein−ligand interactions, *Protein Eng. 8*, 127−134.
43. DeLano, W. L. (2002) The PyMOL Molecular Graphics System, DeLano Scientific, San Carlos, CA.

BI052272Q